Biochemistry and Biophysics Reports 31 (2022) 101300

Contents lists available at ScienceDirect

Biochemistry and Biophysics Reports

journal homepage: www.elsevier.com/locate/bbrep

Polycationic peptide R^7-G-A$\beta_{25\text{-}35}$ selectively induces cell death in leukemia Jurkat T cells through speedy mitochondrial depolarization, and CASPASE-3 -independent mechanism

Miguel Mendivil-Perez, Marlene Jimenez-Del-Rio, Carlos Velez-Pardo *

Grupo de Neurociencias de Antioquia, Instituto de Investigaciones Médicas, Facultad de Medicina, Universidad de Antioquia (UdeA), Calle 70 No. 52-21, Calle 62 # 52-59, Torre 1, Lab 412, Medellin, Colombia

ARTICLE INFO

Keywords:
A$\beta_{25\text{-}35}$
Acute lymphoblastic leukemia
Cationic
Jurkat
Leukemia
Oxidative stress
Synthetic peptide

ABSTRACT

Background: Acute lymphoblastic leukemia (ALL) is still incurable hematologic neoplasia in an important percentage of patients. Therefore, new therapeutic approaches need to be developed.
Methods: To evaluate the cellular effect of cell-penetrating peptides (C-PP) on leukemia cells, Jurkat cells -a model of ALL were exposed to increasing concentration (50–500 μM) Aβ_{25-35}, R^7-G-A$\beta_{25\text{-}35}$ and Aβ_{25-35}-G-R^7 peptide for 24 h. 3-(4,5-dimethylthiazol-2-yl)-2,5-diphenyltetrazolium bromide (MTT) assay, flow cytometry (FC), and fluorescent microscopy (FM) analysis were used to assess metabolic viability, cell cycle and proliferation, mitochondria functionality, oxidative stress, and cell death markers.
Results: We report for the first time that the R^7-G-A$\beta_{25\text{-}35}$, but not Aβ_{25-35} peptide, induced selective cell death in Jurkat cells more efficiently than the Aβ_{25-35}-G-R^7 peptide. Indeed, R^7-G-A$\beta_{25\text{-}35}$ (200 μM) altered the metabolic activity (−25%), arrested the cell cycle in the G2/M-phase (15%), and induced a significant reduction of cellular proliferation (i.e., −74% reduction of Ki-67 nuclei reactivity). Moreover, R^7-G-A$\beta_{25\text{-}35}$ induced the dissipation of mitochondrial membrane potential ($\Delta\Psi_{m,}$ 51%) and produced an important amount of reactive oxygen species (ROS, 75% at 8 h) in Jurkat cells. The exposure of cells to antioxidant/cytoprotectant N-acetylcysteine (NAC) did not prevent R^7-G-A$\beta_{25\text{-}35}$ from a loss of $\Delta\Psi_m$ in Jurkat cells. The peptide was also unable to activate the executer CASPASE-3, thereby preserving the integrity of the cellular DNA corroborated by the fact that the caspase-3 inhibitor NSCI was unable to protect cells from R^7-G-A$\beta_{25\text{-}35}$ -induced cell damage. Further analysis showed that the R^7-G-A$\beta_{25\text{-}35}$ peptide is specifically localized at the outer mitochondria membrane (OMM) according to colocalization with the protein translocase TOMM20. Additionally, the cytotoxic effect of the poly-R^7 peptide resembles the toxic action of the uncoupler FCCP, mitocan oligomycin, and rotenone in Jurkat cells. Importantly, the R^7-G-A$\beta_{25\text{-}35}$ peptide was innocuous to menstrual mesenchymal stromal cells (MenSC) –normal non-leukemia proliferative cells.
Conclusion: Our findings demonstrated that the cationic Aβ peptide possesses specific anti-leukemia activity against Jurkat cells through oxidative stress (OS)- and CASPASE-3-independent mechanism but fast mitochondria depolarization.

1. Introduction

Acute lymphoblastic leukemia (ALL) is a malignant transformation and proliferation of either B-cell or T-cell lymphoid progenitor cells in the bone marrow, blood, and extramedullary sites affecting children, young adolescents, and adults [1] around the world [2]. According to the American Cancer Society, there are approximately 5690 new cases of ALL, and about 1580 deaths in 2021. While childhood ALL studies have shown improved 5-year overall survival (OS) rates exceeding 90% [3], only 30–40% of adult patients with ALL will achieve long-term remission [4]. Although conventional cytotoxic chemotherapy [5,6] or in combination with monoclonal antibodies (e.g., Ref. [7]) used to treat ALL results in high cure rates, treatment is suboptimal in an important percentage of pediatric and adult patients with relapsed and refractory

* Corresponding author.
E-mail addresses: miguel.mendivil@udea.edu.co (M. Mendivil-Perez), marlene.jimenez@udea.edu.co (M. Jimenez-Del-Rio), calberto.velez@udea.edu.co (C. Velez-Pardo).

https://doi.org/10.1016/j.bbrep.2022.101300
Received 29 April 2022; Received in revised form 26 May 2022; Accepted 13 June 2022

ALL. Therefore, new treatment options are needed for the treatment of resistance ALL. Indeed, leukemia cells avoid apoptosis -a regulated form of cell death [8] contributing to their pathological features. Since apoptosis can be initiated through the intrinsic pathway that depends on mitochondrial outer membrane permeabilization or the extrinsic pathway that depends on external signals via cell receptors [9], a reasonable strategy would be to trigger apoptosis by agents that directly or indirectly target mitochondria or by external signals to boost cell death for anti-leukemic therapy.

Polycationic peptides are a large class of short amino acid sequences (5–30 residues) composed mainly of multiple lysines (K) and/or arginine (R) residues usually used as anti-microbial agents (e.g., Refs. [10–14]). It is the cationic properties that promote the preferential binding of peptides to the negatively charged bacterial cytoplasmic membrane instead of the zwitterionic membrane of mammalian cells [15]. Interestingly, not only they can impair microbial cell walls and plasma membrane phospholipids but also mitochondria in free-cell assays [16,17]. Currently, polycationic peptides have appeared as specifically anti-cancer therapeutic agents [18], targeting mitochondria acting as class 6 mitocan agents [19,20]. Since R oligomers have been shown to facilitate cellular uptake of cargo proteins [21] probably through membrane multilamellar and subsequently entrance via formation of a fusion pore [22], thereby enhancing their capacity to directly permeabilize mitochondria (e.g., Ref. [23]). Indeed, synthetic cell-penetrating peptides **(**C-PP**)** poly-R^n ($n > 6$) have currently been used as the delivery vector [24,25]. For instance, the peptide r7-kla (D-hepta-arginine linked to D-forms of KLA) induced apoptosis (48%) in leukemia Jurkat cells -a T-cell ALL line [23]. Moreover, it has been shown that cationic peptides such as P7-4 (R^7-GG-IYLATALAKWALKQGF) and P7-5 (IYLATALAKWALKQGF-GG-R^7) significantly induced demise (29% and 31%, respectively) of leukemia Jurkat cells [17]. Taken together these data suggest that some poly-R^n-spacer-cargo peptides provoke apoptosis in leukemia cells mainly through targeting the mitochondrial membrane.

The $A\beta_{25-35}$ with sequence GSNKGAIIGLM is an eleven-residue peptide produced by proteolytic conversion of racemized β-amyloid ([d-Ser^{26}] $A\beta_{1-40}$) in the brains of aged Alzheimer's disease patients [26]. Since the $A\beta_{25-35}$ peptide is amphiphilic and tends to aggregate, it has been shown that the peptide displays neurotoxic properties [27] probably through disruption of the structure of the plasma membrane causing uncontrollable permeation of Ca^{2+} ions [28]. However, no data are available to establish whether $A\beta_{25-35}$ peptide might be cytotoxic to other non-neuronal cells. Based on the above information, we used $A\beta_{25-35}$ as a paradigm peptide. Indeed, the C-PP vector R^7 was fused to $A\beta_{25-35}$ at their N- or C-termini through one unstructured glycine residue used as a spacer to obtain R^7-G-$A\beta_{25-35}$ and $A\beta_{25-35}$-G-R^7, respectively. We hypothesized that $A\beta_{25-35}$ peptide induces apoptosis in leukemia cells. We also theorized that either R^7-G-$A\beta_{25-35}$ or $A\beta_{25-35}$-G-R^7 increase several folds apoptosis when compared to $A\beta_{25-35}$ peptide. To test these hypotheses, we used Jurkat T cell to elucidate the molecular mechanism of cell death induced by either cationic $A\beta_{25-35}$ or non-cationic $A\beta_{25-35}$ peptides. To test the selectivity of peptides to induce cell death, menstrual-derived mesenchymal stromal cells (MenSCs) were used as control. We report for the first time that the R^7-G-$A\beta_{25-35}$, but not $A\beta_{25-35}$ peptide, induced selective cell death in Jurkat cells more efficiently than the $A\beta_{25-35}$-G-R^7 peptide. The R^7-G-$A\beta_{25-35}$ peptide altered several metabolic parameters in the leukemia cell line such as metabolic activity, cell cycle, cellular proliferation, $\Delta\Psi_m$ leading to cell death by a mechanism independent of oxidative stress (OS) and CASPASE-3 activation but fast mitochondrial depolarization. Our findings suggest the cationic Aβ peptide possesses anti-leukemia activity against ALL.

2. Materials and methods

2.1. Peptide synthesis

Peptide $A\beta_{25-35}$-G-R^7 was synthetized by Dr. F Guzman (Núcleo Biotecnología Curauma, Valparaíso, Chile). Peptide synthesis was performed in a Liberty BlueTM automated microwave peptide synthesizer (CEM Corp., Matthews, NC, USA) following a standard fluorenylmethoxycarbonyl protecting group (Fmoc)/tert-butyl-L-tyrosine (*t*Bu) protocol as previously described [29]. Briefly, a Rink Amide AM resin (loading 0.6 mmol/g) was used as the solid support. Standard couplings of amino acids were carried out at 0.2 M in dimethylformamide (DMF) using diisopropylcarbodiimide (DIC)/OxymaPure® activation (the synthesis method optimization according to Liberty BlueTM recommended operation (CEM Corp., Matthews, NC, (USA)), and the corresponding amino acid. Fmoc removal was done with three different reagents: 20% v/v 4-methylpyrazole (4 MP) in DMF; 20% v/v. Deprotection and coupling were performed as described [29]. For arginine, an additional coupling step was performed. Once synthesis was complete, peptides were cleaved manually from the resin with trifluoroacetic acid (TFA) under gentle agitation for 4 h at room temperature (r.t.) in the presence of scavengers (standard cleavage solution: TFA/tri-isopropylsilane (TIS)/Water 95:2.5:2.5). After filtration, the crude peptide was precipitated by cold diethyl ether, centrifuged, washed with cold Et2O five times, dried, dissolved in ultrapure water, frozen, and lyophilized. Peptide R^7-G-$A\beta_{25-35}$ was synthesized by Dr. S Estrada-Gomez and CF Salinas-Restrepo (Ofidism/Escorpionism Program, Universidad de Antioquia). The peptide was chemically synthesized through the solid phase using Fmoc/*t*Bu as the orthogonal protection strategy in the Rink AM resin using the simultaneous synthesis strategy described in Ref. [30]. The (Benzotriazole-1-yl) tetramethyluronium hexafluorophosphate (HBTU), (Benzotriazolyl) tetramethyluronium tetrafluoroborate (TBTU), DIC, and O-(6-Chloro-1-hydrocibenzotriazol-1-yl)-1,1,3,3-tetramethyluronium tetrafluoroborate (TCTU) were used as activators, and the deprotection was carried away with piperidine 20% in DMF. For the cleavage a 92.5% TFA, 2.5% TIS, 2.5% 2-mercaptoethanol and 2.5% water solution was used as described in Ref. [29]. The crude and folded peptide was solubilized in 200 μL of solution A (0.1% TFA in water) and centrifuged at 1.000 g for 3 min. The supernatant was applied to a reverse-phase CNW Athena C18-WP (CNW Technologies, Düsseldorf, Germany) column (4.6 × 100 mm, 5 μm, 100 Å), and separated by RP-HPLC on a Shimadzu Prominence chromatograph (Kyoto, Japan). The crude peptide was precipitated by cold diethyl ether, centrifuged, washed with cold Et2O three times, dried, dissolved in ultrapure water, frozen, and lyophilized. All reactants were from Merck Millipore (Merck Millipore, Billerica, MA, USA). Peptide $A\beta_{25-35}$ was acquired from Sigma-Aldrich (Cat#A4559). For culture experiments, peptides were resuspended in Roswell Park Memorial Institute (RPMI)-1640 culture medium with glucose (11 mM; Gibco/Invitrogen, Grand Island, New York, USA).

2.2. Cell line and reagents

Jurkat clone E6-1 cells (Catalog no. TIB-152; American Type Culture Collection (ATCC), Manassas, Virginia, USA) were cultured according to the supplier's indications. The cell suspension ($1x10^6$ cells/well in 1 mL final volume) was exposed to increasing concentrations of synthetic peptides (0–500 μM) freshly prepared in RPMI-1640 medium with glucose (11 mM; Gibco/Invitrogen, Grand Island, New York, USA) in the absence or presence of different products of interest (e.g., antioxidant, inhibitors) for 24 h at 37 °C. All other reagents were from Sigma-Aldrich (St Louis, Missouri, USA).

2.3. Isolation of mesenchymal stromal cells (MSCs)

Isolation of MenSCs was performed according to previous reports [31]. Briefly, a menstrual blood sample (**t**issue **b**ank **c**ode (TBC # 69308) was delivered to the laboratory and mixed with an equal volume of phosphate buffer saline (PBS) containing 1 mM ethylenediamine tetra-acetic acid (EDTA), with 100 U/mL penicillin/streptomycin 0.25 mg/mL amphotericin B, and standard Ficoll procedures. After centrifugation, the cells were suspended in a buffy coat and were transferred into a new tube, washed in PBS twice, and resuspended in a growth medium (low-glucose Dulbecco's modified Eagle's medium (DMEM) medium supplemented with 10% fetal bovine serum (FBS, Gibco, USA), 100 U/mL penicillin/streptomycin, and 0.25 mg/mL amphotericin B), and seeded into 25-cm^2 plastic cell culture flasks at 37 °C with 5% humidified CO_2.

2.4. MTT assay

The proliferation of Jurkat cells was evaluated using the 3-(4,5-dimethylthiazol-2-yl)-2,5-diphenyltetrazolium bromide (MTT) assay by determining the conversion of the water-soluble MTT to an insoluble formazan [32]. Briefly, cells were pelleted and were incubated under increasing (0–500 μM) concentrations of synthetic peptides for 24 h. Thereafter, the medium was removed and replaced with fresh medium without phenol red. Cells were incubated with 1.2 mM MTT at 37 °C for 3 h and after incubated with dimethyl sulfoxide (DMSO). Finally, samples were mixed, and the absorbance was read at 570 nm using a Stat Fax 3200 microplate spectrophotometer (Awareness Technology, Palm City, Florida, USA). MTT absorbance was assessed 3 times in independent experiments.

2.5. Ki-67 immunofluorescence

To evaluate the effect of synthetic peptides on Jurkat cells proliferation, we evaluated the percentage of Ki-67 positive nuclei according to Ref. [33]. Briefly, the treated cells were fixed with cold ethanol (−20 °C) for 20 min followed by 10% bovine serum albumin (BSA) blockage. Thereafter, cells were incubated overnight with anti-Ki-67 monoclonal mouse antibody conjugated with fluorescein isothiocyanate isomer 1 (FITC, Cat #F0788, Dako) 1:200. The nuclei were stained with 1 μM Hoechst 33342 (life technologies). Ki-67 reactivity was quantified in a Zeiss Axiostart 100 Fluorescence Microscope equipped with a Zeiss AxioCam Cm1 (Zeiss Wöhlk-Contact-Linsen, Gmb Schcönkirchen, Germany) by assessing the labeling percentage from the ratio of the number of nuclei-stained Ki-67 to the total number of nuclei counted per section. At least 10 different randomly selected areas were counted.

2.6. Determination of DNA fragmentation and cell cycle by flow cytometry

DNA fragmentation and cell cycle were determined by using a hypotonic solution of propidium iodide (PI, [34]). After treatments, cells ($1x10^5$) were washed with PBS (pH 7.2) and stored in 95% ethanol overnight at −20 °C. Thereafter, cells were washed and incubated in a 400 μL solution containing PI (50 μg/ml), RNase A (100 μg/mL), EDTA (50 mM), triton X-100 (0.2%) for 30 min at 37 °C. The cell suspension was analyzed for PI fluorescence by using a BD LSRFortessa II flow cytometer (BD Biosciences). Quantitative data and figures were obtained using FlowJo 7.6.2 Data Analysis Software. Cells entering the sub-G1 phase were used as a marker of apoptosis (DNA fragmentation). For cell cycle analysis, the sub-G1 population was subtracted from the total acquired events, and the Dean Jett Fox analysis was applied (root mean square (RMS) < 10). The experiment was conducted three times, and 10, 000 events were acquired for analysis.

2.7. Evaluation of intracellular hydrogen peroxide (H_2O_2) by flow cytometry

H_2O_2 was determined with 2′,7’ -dichlorofluorescein diacetate (0.5 μM, $DCFH_2$-DA) according to Ref. [35]. Briefly, after cell treatment with compounds of interest, cells (1×10^5) were incubated with $DCFH_2$-DA reagent for 30 min at 37 °C in the dark. Cells were washed and dichlorofluorescein (DCF) fluorescence was determined using a BD LSRFortessa II flow cytometer (BD Biosciences). The experiment was conducted three times, and 10,000 events were acquired for analysis. Quantitative data and figures were obtained using FlowJo 7.6.2 Data Analysis Software.

2.8. Analysis of mitochondrial membrane potential ($\Delta\Psi_m$) by flow cytometry

Assessment of the $\Delta\Psi_m$ was performed according to Ref. [36]. We incubated cells ($1x10^5$) for 20 min at r. t. in the dark with a deep red mitotracker (20 nM final concentration) compound (Thermo Scientific, cat# M22426). Cells were analyzed by using a BD LSRFortessa II flow cytometer (BD Biosciences). The experiment was conducted three times, and 10,000 events were acquired for analysis. Quantitative data and figures were obtained using FlowJo 7.6.2 Data Analysis Software.

2.9. Assessment of cell death by fluorescent microscopy

MenSC and Jurkat cells were incubated under increasing (0–500 μM) concentrations of synthetic peptides for 24 h. Nuclei were stained for 20 min at 37 °C in the dark with Hoechst 33342 (0.5 μM), deep red mitotracker (20 nM), and $DCFH_2$-DA, (0.5 μM). Thereafter, cells were deposited in a microscope slide and covered with a coverslip. Fluorescence microscopy analysis was performed with a Zeiss Axiostart 100 fluorescence microscope equipped with a Zeiss AxioCam Cm1 (Zeiss Wöhlk-Contact-Linsen, Gmb Schcönkirchen, Germany). The adjustment of the images obtained was performed with the software provided by the manufacturer (ZEN 2 Core).

2.10. Antioxidant and pharmacological inhibitor protection experiments

Jurkat cell suspension ($1x10^6$/well in 1 ml final volume) was left untreated or treated with R^7-G-A$\beta_{25\text{-}35}$ synthetic peptide (200 μM) alone or in combination with either antioxidant N-acetyl-L-cysteine (NAC, 1 mM) or the caspase-3 inhibitor 1-(4-Methoxybenzyl)-5-[2-(pyridin-3-yloxymethyl)pyrrolidine-1-sulfonyl]-1H-indole-2,3-dione (NSCI, 10 μM, Sigma-Aldrich, catalog N1413) at 37 °C for 24 h. The cells were evaluated for $\Delta\Psi_m$ by flow cytometry. The assessment was repeated three times in independent experiments.

2.11. Flow cytometry analysis for CASPASE-3

Flow cytometry acquisition was used to determine the percentage of Caspase-3 positive cells according to Ref. [37]. Jurkat cells were treated according to the above-mentioned procedures. The fixated Jurkat cells were washed and incubated with rabbit anti-Caspase-3 (Millipore, cat #AB3623) primary antibody (1:200) at 4 °C overnight. Cell suspensions were washed and incubated with DyLight 488 donkey anti-rabbit antibody (1:500). Finally, cells were washed and re-suspended in PBS for analysis on a BD LSRFortessa II flow cytometer (BD Biosciences). Twenty thousand events were acquired, and the acquisition analysis was performed using FlowJo 7.6.2 Data Analysis Software.

2.12. Analysis of mitochondrial membrane potential by fluorescent microscopy

The $\Delta\Psi$m was evaluated according to Ref. [38]. Briefly, we incubated cells ($1 \text{ x } 10^5$) for 20 min at 37 °C in the dark with cationic and lipophilic 3,3′-dihexyloxacarbocyanine iodide ($DiOC_6(3)$), 20 nM final concentration compound (Calbiochem, Darmstadt, Germany; cat # D-273). Cells were incubated with mitochondrial-targeted drugs (i.e., carbonyl cyanide 4-(trifluoromethoxy)phenylhydrazone, FCCP, 10 μM), oligomycin (5 μg/ml), rotenone (100 μM)) or R^7-G-A$\beta_{25\text{-}35}$ peptide (200 μM) for 0, 30, 60, 120 and 240 s. Fluorescence microscopy analysis was performed with a Zeiss Axiostart 50 Fluorescence Microscope equipped with a Zeiss AxioCam Cm1 (Zeiss Wöhlk-Contact-Linsen, Gmb Schcönkirchen, Germany). The adjustment of the images and the spectral images were obtained with the software provided by the manufacturer (ZEN 2 Core). The experiment was conducted three times.

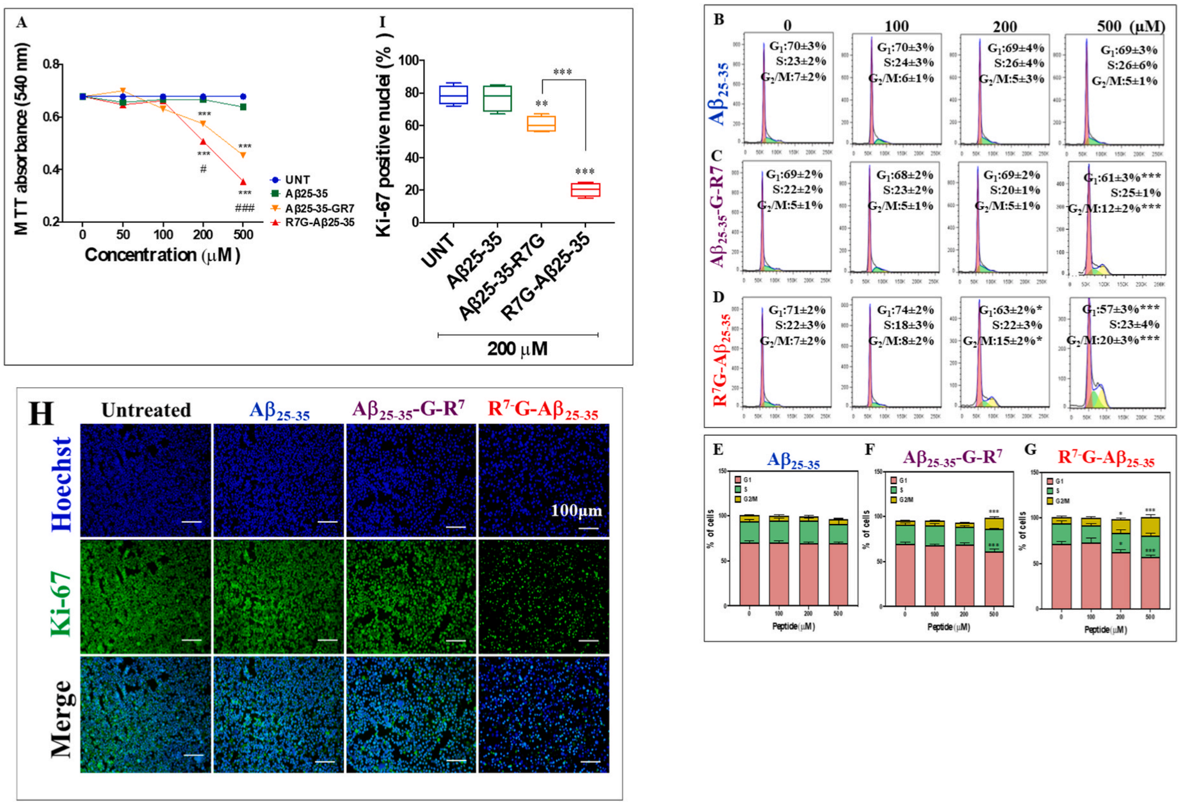

Fig. 1. Effect of Aβ$_{25\text{-}35}$, Aβ$_{25\text{-}35}$-G-R^7, and R^7-G-Aβ$_{25\text{-}35}$ synthetic peptides on the metabolic viability, cell cycle, and proliferation in Jurkat cells. (**A**) Cells were left untreated or treated with Aβ$_{25\text{-}35}$, Aβ$_{25\text{-}35}$-G-R^7, and R^7-G-Aβ$_{25\text{-}35}$ (0–500 μM; 24 h), and metabolic viability was measured by MTT assay. (**B-D**) Representative histograms show cell cycle phase in Jurkat cells treated with 0, 100, 200, and 500 μM of Aβ$_{25\text{-}35}$ **(B)**, Aβ$_{25\text{-}35}$-G-R^7 **(C)**, and R^7-G-Aβ$_{25\text{-}35}$ **(D)** synthetic peptides for 24 h. **(E-G)** Quantitative data show the cell cycle phase mean percentage of Jurkat cells treated with 0, 100, 200, and 500 μM of Aβ$_{25\text{-}35}$ **(E)**, Aβ$_{25\text{-}35}$-G-R^7 **(F)**, and R^7-G-Aβ$_{25\text{-}35}$ **(G)** synthetic peptides. **(H)** Representative immunofluorescence images show the Ki-67 and nuclei staining in cells untreated or treated with Aβ$_{25\text{-}35}$, Aβ$_{25\text{-}35}$-G-R^7, and R^{7}G-Aβ$_{25\text{-}35}$ (200 μM) synthetic peptides. **(I)** Quantitative data show the mean percentage of Ki-67 positive nuclei in Jurkat cells untreated or treated with Aβ$_{25\text{-}35}$, Aβ$_{25\text{-}35}$-G-R^7, and R^7-G-Aβ$_{25\text{-}35}$ (200 μM) synthetic peptides. Figures represent 1 out of 3 independent experiments. The numbers represent the mean percentage of three independent experiments. *$*p<0.05$; $**p<0.01$; $***p<0.001$.* Image magnification 20x.

2.13. Immunofluorescence colocalization analysis of the Aβ peptide and cluster of differentiation (CD)45 or translocase of the outer mitochondrial membrane (TOMM)20

The immunofluorescent staining procedure was according to the standard procedure [39]. Briefly, untreated, and treated cells (0 or 200 μM, respectively) with synthetic peptides (Aβ$_{25\text{-}35}$, R^7-G- Aβ$_{25\text{-}35}$) were plated in a positively charged slide and air-dried. Cells were fixed using 4% formaldehyde for 20 min. After permeabilization, cells were incubated overnight at 4 °C with primary anti-β-amyloid (25–35) rabbit polyclonal antibody (GenScript, cat# A00687-40), in combination with CD45 mouse monoclonal antibody (BD Pharmingen, cat# 555482) or TOMM20 mouse monoclonal antibody (ab115746). All primary antibodies were prepared at 1:200. After several washes, cells were incubated with Alexa Fluor488 and 594 donkey anti-rabbit and anti-mouse IgG secondary antibodies, respectively (Life Technologies), according to the supplier's protocol (Life Technologies, Eugene, Oregon, USA).

2.14. Photomicrography and image analysis

The fluorescent microscopy photographs were taken using a Zeiss Axiostart 100 Fluorescence Microscope equipped with a Zeiss AxioCam Cm1 (Zeiss Wöhlk-Contact-Linsen, Gmb Schönkirchen, Germany). Images were analyzed by ImageJ software [40]. The figures were transformed into 8-bit images and the background was subtracted. The cellular measurement regions of interest (ROI) were drawn over cell structures (i.e., membrane or mitochondria) and the fluorescence intensity was subsequently determined by applying the same threshold for controls and treatments.

2.15. Statistical analysis

Statistical analyses were performed using the GraphPad Prism 6 scientific software (GraphPad, Software, Inc. La Jolla, CA, USA). Data are expressed as the mean ± S.D. of a minimum of three independent experiments. One-way ANOVA with a Tukey post hoc test was used to compare the differences between the experimental groups. A P-value <0.05 (*), <0.01 (**) and <0.001 (***) were statistically significant.

3. Results

3.1. R^7-G-Aβ$_{25\text{-}35}$ and Aβ$_{25\text{-}35}$-G-R^7, but not Aβ$_{25\text{-}35}$ peptide, induce cell cycle arrest, reduce cellular proliferation, and diminish cellular metabolic activity in Jurkat cells

We first wanted to evaluate the effect of Aβ$_{25\text{-}35}$, R^7-G-Aβ$_{25\text{-}35}$, and Aβ$_{25\text{-}35}$-G-R^7 peptides on cellular metabolic activity, cell proliferation, and cell cycle in Jurkat cells. To this aim, cells were left untreated or treated with an increasing concentration of the peptides (0–500 μM) for 24 h. As shown in Fig. 1A, Jurkat cells exposed to Aβ$_{25\text{-}35}$ peptide remain unaffected according to cellular metabolic activity assay when compared to untreated cells. However, leukemia cells showed a progressive and significant concentration-dependent viability loss by both R^7-G-Aβ$_{25\text{-}35}$ (e.g., −25, −48% reduction at 200–500 μM, respectively)

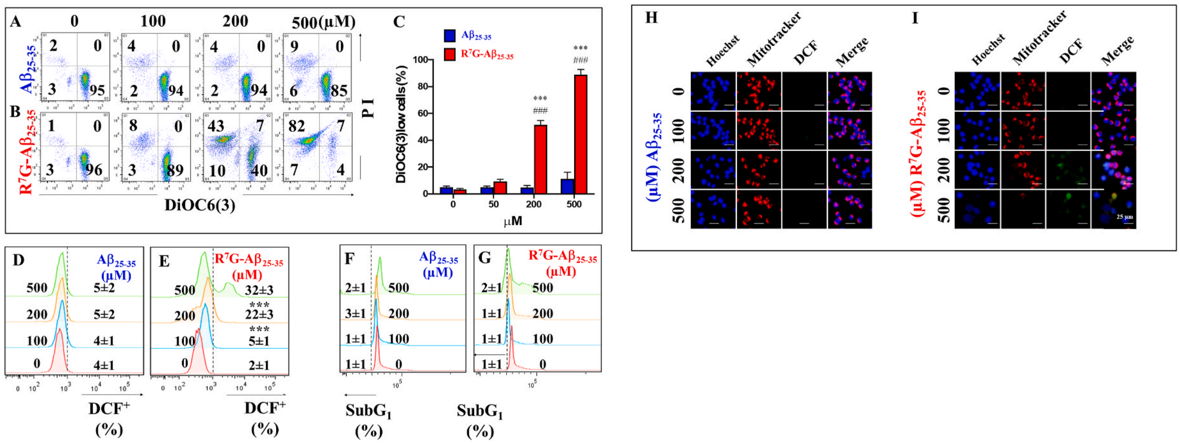

Fig. 2. Synthetic peptide R^7-G-Aβ$_{25\text{-}35}$ induces dissipation of mitochondrial membrane potential (ΔΨm), and production of reactive oxygen species (ROS), but no damage to nuclei in Jurkat cells.
(A-I) Representative dot plot figures show DiOC$_6$(3)/PI double staining in Jurkat cells treated with 0, 100, 200, and 500 μM **(A)** Aβ$_{25\text{-}35}$, and **(B)** R^7-G-Aβ$_{25\text{-}35}$ synthetic peptides for 24 h. **(C)** Quantitative data showthe DiOC$_6$(3)^{low} mean percentage (Q1 + Q4) of Jurkat cells treated with 0, 100, 200, and 500 μM Aβ$_{25\text{-}35}$ and R^7-G-Aβ$_{25\text{-}35}$ synthetic peptides. Representative histograms show the DCF $^+$ mean percentage in Jurkat cells treated with 0, 100, 200, and 500 μM **(D)** Aβ$_{25\text{-}35}$ and **(E)** R^7-G-Aβ$_{25\text{-}35}$ peptides. Representative histograms show the Sub-G$_1$ mean percentage in Jurkat cells treated with 0, 100, 200, and 500 μM **(F)** Aβ$_{25\text{-}35}$ and **(G)** R^7-G-Aβ$_{25\text{-}35}$ peptides. Representative fluorescence images show the Hoechst/Mitotracker/DCF triple staining in cells treated with 0, 100, 200, and 500 μM **(H)** Aβ$_{25\text{-}35}$ and **(I)** R^7-G-Aβ$_{25\text{-}35}$ peptide. Figures represent 1 out of 3 independent experiments. The numbers represent the mean percentage of three independent experiments. *$^*p<0.05$; $^{**}p<0.01$; $^{***}p<0.001$.* Image magnification 20x.

and Aβ$_{25\text{-}35}$-G-R^7 (e.g., -15 -33%) peptides. Importantly, R^7-G-Aβ$_{25\text{-}35}$ significantly reduced cellular metabolic activity compared to the Aβ$_{25\text{-}35}$-G-R^7 peptide. Cell cycle analysis revealed that Aβ$_{25\text{-}35}$ did not affect the Jurkat cell cycle (Fig. 1B and E), whereas Aβ$_{25\text{-}35}$-G-R^7 (Fig. 1C and F) and R^7-G-Aβ$_{25\text{-}35}$ (Fig. 1D and G) induced a significant G$_2$/M-phase cell arrest in a concentration-dependent manner, albeit R^7-G-Aβ$_{25\text{-}35}$ (200 μM) was more effective altering the Jurkat cell cycle than the Aβ$_{25\text{-}35}$-G-R^7 peptide. Similarly, we found that Aβ$_{25\text{-}35}$ peptide (e.g., 200 μM) did not affect proliferative-associated Ki-67 protein expression (Fig. 1H and I), whereas R^7-G-Aβ$_{25\text{-}35}$ peptide (e.g., 200 μM) and Aβ$_{25\text{-}35}$-G-R^7 induced a significant reduction (−74% and -23%) of Ki-67 nuclei reactivity, respectively (Fig. 1I). Because the R^7-G-Aβ$_{25\text{-}35}$ peptide altered cellular metabolic activity, cell proliferation, and cell cycle more efficiently than Aβ$_{25\text{-}35}$-G-R^7 in Jurkat cells, the former peptide was selected for further experiments. The Aβ$_{25\text{-}35}$ peptide was included for comparative purposes.

3.2. R^7-G-Aβ$_{25\text{–}35}$, but not Aβ$_{25\text{-}35}$ peptide, induces dissipation of mitochondrial membrane potential (ΔΨm) and produced reactive oxygen species (ROS) preserving cellular DNA integrity in Jurkat cells

Next, we wanted to determine whether the synthetic peptides induce ΔΨm, ROS production, and DNA fragmentation in leukemic cells. Therefore, Jurkat cells were left untreated or treated with increasing concentrations (0–500 μM) of Aβ$_{25\text{-}35}$, or R^7-G-Aβ$_{25\text{-}35}$ for 24 h at 37 °C. As shown in Fig. 2, Aβ$_{25\text{-}35}$ neither alter the ΔΨ$_m$ (Fig. 2A and C) nor influenced ROS production (Fig. 2D) nor induced DNA fragmentation (Fig. 1F), whereas R^7-G-Aβ$_{25\text{-}35}$ peptide not only significantly induced a concentration-dependent loss of ΔΨm (Fig. 2B and C) but induced ROS production (Fig. 2E) according to flow cytometry analysis. These observations were confirmed by fluorescent microscopy (Fig. 2H and I). Analysis of the content of cellular DNA indicated that SubG$_1$ remained unaffected when exposed to either peptide (Fig. 2F and G).

3.3. The toxic effect of the R^7-G-Aβ$_{25\text{-}35}$ peptide is independent of ROS production and CASPASE-3 activation in Jurkat cells

Since ROS plays an important role as a signaling molecule [41], we evaluated whether the generation of ROS by R^7-G-Aβ$_{25\text{-}35}$ peptide-induced activation of CASPASE-3 over time. As shown in Fig. 3, R^7-G-Aβ$_{25\text{-}35}$ induced a dramatic increment of ROS production up to 8 h (i.e., ~**73%** increase) followed by a significant reduction (e.g., ~ −71% reduction) after 24 h according to DCFH$_2$-DA oxidation into DCF fluorescence assay (Fig. 3A). CASPASE-3 activity remained unaffected during observational time points (Fig. 3B). To further corroborate these observations, we left Jurkat cells untreated or treated with R^7-G-Aβ$_{25\text{-}35}$ peptide alone or in combination with NAC – a well-known cytoprotective and antioxidant agent [42,43], or NSCI -a caspase-3 inhibitor. Fig. 3 shows that neither NAC (5 mM) nor NSCI (10 μM) protected Jurkat cells against R^7-G-Aβ$_{25\text{-}35}$ peptide-induced loss of ΔΨm (Fig. 3C and D).

3.4. The R^7-G-Aβ$_{25\text{-}35}$ peptide dramatically reduces ΔΨ$_m$ by its mitochondrial accumulation in Jurkat cells

To further characterized the effect of the R^7-G-Aβ$_{25\text{-}35}$ peptide on mitochondria, we wanted to specifically localize the cellular site of action of the peptide. To this aim, we left Jurkat cells untreated or treated with Aβ$_{25\text{-}35}$ or R^7-G-Aβ$_{25\text{-}35}$ peptides for 24 h. Thereafter, we used the plasma membrane marker CD45, or outer mitochondrial membrane receptor TOMM20 together with antibody Aβ$_{25\text{-}35}$ for co-localization purposes. As shown in Fig. 4, Aβ$_{25\text{-}35}$ localizes neither at the plasma membrane (Fig. 4B, i.e., positive CD45 /negative Aβ$_{25\text{-}35}$ fluorescence) nor at mitochondria (Fig. 4E, i.e., positive TOMM20/negative Aβ$_{25\text{-}35}$ fluorescence) compared to untreated cells (Fig. 4A and D), whereas R^7-G-Aβ$_{25\text{-}35}$ peptide was positively detected at mitochondria (Fig. 4C, 4F–H).

3.5. The R^7-G-Aβ$_{25\text{-}35}$ peptide induces a rapid loss of ΔΨm by affecting mitochondria oxidative phosphorylation and uncoupling mitochondrial potential in Jurkat cells

The above observations prompted us to evaluate the effect R^7-G-Aβ$_{25\text{-}35}$ peptide on the mitochondria in Jurkat cells over time. Flow cytometry analysis indicates that R^7-G-Aβ$_{25\text{-}35}$ peptide significantly reduced the ΔΨm as early as 4 h in Jurkat cells (Fig 5A, 50%= 37% early (green circle, Q4) plus 13% late (orange circle, Q1) mitochondrial

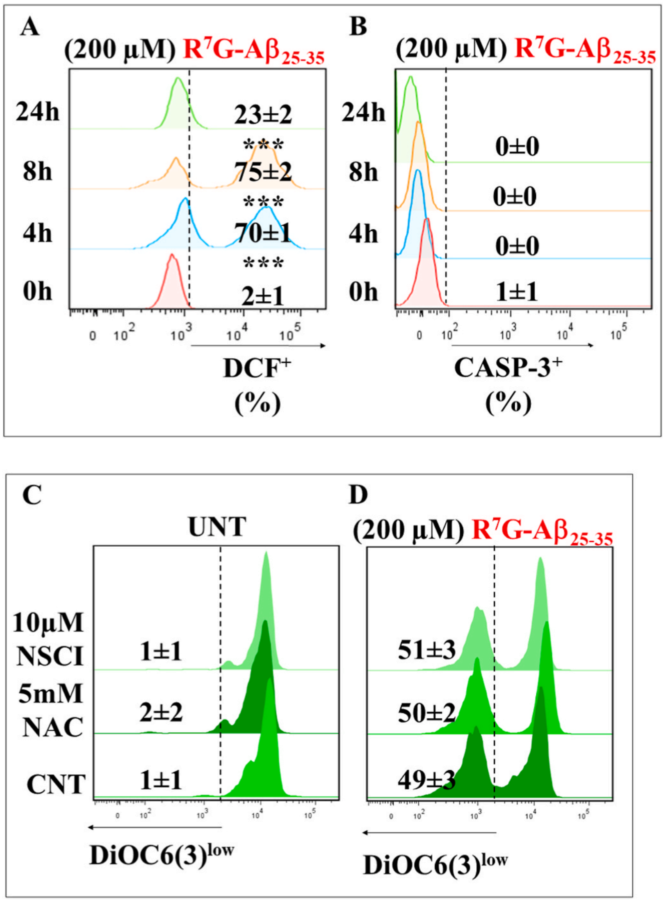

Fig. 3. Synthetic peptide R^7-G-A$\beta_{25\text{-}35}$ induces cell death in a CASPASE-3 (CASP-3)- and reactive oxygen species-independent mechanism in Jurkat cells

(A) Representative histograms show the DCF $^+$ mean percentage in Jurkat cells treated with R^7-G-A$\beta_{25\text{-}35}$ peptide (200 μM) for 0, 4, 8, and 24 h. **(B)** Representative histograms show the CASP-3$^+$ mean percentage of Jurkat cells treated with R^7-G-A$\beta_{25\text{-}35}$ (200 μM) peptide for 0, 4, 8, and 24 h. **(C)** Representative histograms show the DiOC$_{(6)}$3^{low} mean percentage of Jurkat cells untreated, or with NSCI (10 μM) or NAC (5 mM) only for 24 h. **(D)** Representative histograms show the DiOC$_6$(3)^{low} mean percentage of Jurkat cells treated with R^7-G-A$\beta_{25\text{-}35}$ peptide (200 μM) only or with NSCI (10 μM) or with NAC (5 mM) for 24 h. The numbers represent the mean percentage of three independent experiments. *$p<0.05$; **$p<0.01$; ***$p<0.001$.

damage), and this effect was stable over time up to 24 h (~**50%**, Fig. 5B) followed by a stepwise progressive cell membrane permeabilization according to propidium iodide-stained cells (Fig. 5A). We wanted to determine whether the R^7-G-A$\beta_{25\text{-}35}$ peptide was linked to the impairment of the mitochondria oxidative phosphorylation constituents. To this aim, we compared the effect of R^7-G-A$\beta_{25\text{-}35}$ peptide with other well-known mitochondrial-targeted drugs such as mitochondria Complex I (NADH: ubiquinone oxidoreductase) inhibitor rotenone (class 5 mitocan), complex V (ATP synthase) inhibitor oligomycin (class 5 mitocan), and classical uncoupler of oxidative phosphorylation FCCP (carbonyl cyanide 4-(trifluoromethoxy) phenylhydrazone) reflected as ΔΨm changes on Jurkat cells. As expected, in about 240 s, FCCP (Fig. 5C), oligomycin (Fig. 5D), and rotenone (Fig. 5E) induced a rapid and progressive loss of ΔΨm according to DiOC$_6$(3) fluorescence change analysis (Fig. 5G). Strikingly, R^7-G-A$\beta_{25\text{-}35}$ peptide -a class 6 mitocan had a similar effect on the $\Delta\Psi_m$ when compared to mitochondrial-targeted drugs (Fig. 5F and G).

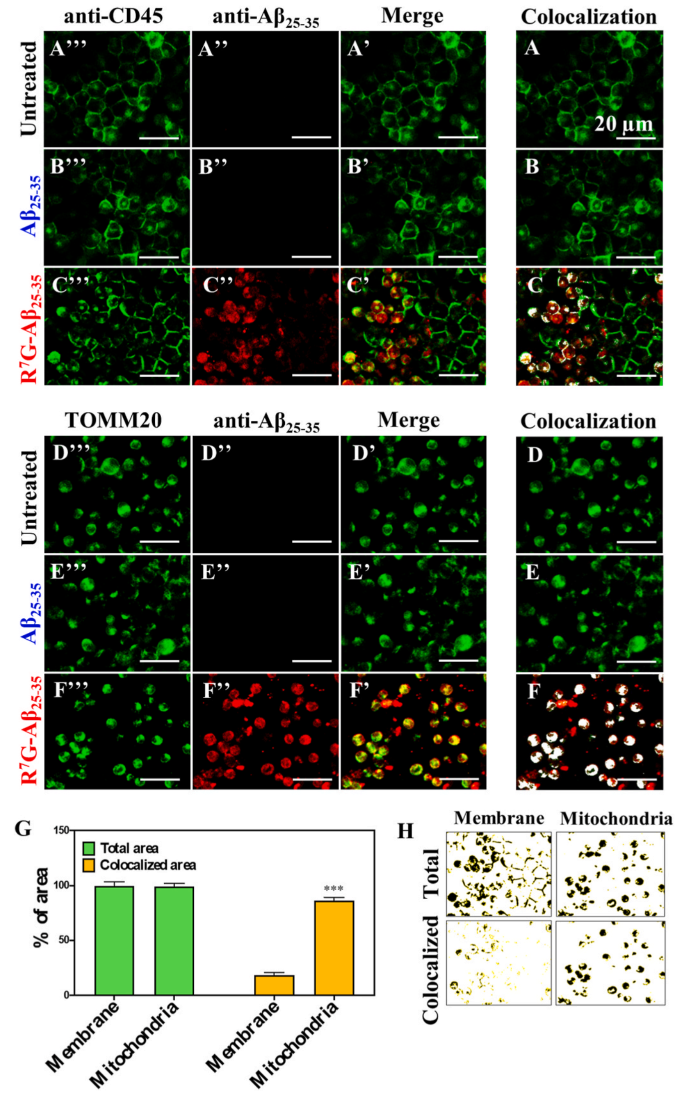

Fig. 4. Synthetic peptide R^7-G-A$\beta_{25\text{-}35}$ co-localizes with mitochondria but not with the cell membrane in Jurkat cells.

(A-C) Representative colocalization images **(A-C)** and merge images **(A′-C′)** show A$\beta_{25\text{-}35}$ epitope sequence **(red; A″-C″)** and CD45 **(green; A‴-C‴)** of untreated **(A)**, treated with A$\beta_{25\text{-}35}$ **(B)** or with R^7-G-A$\beta_{25\text{-}35}$ peptide **(C)** in Jurkat cells for 24 h. **(D-F)** Representative colocalization images **(D-F)** and merge images **(D′-F′)** show A$\beta_{25\text{-}35}$ epitope sequence **(red; D″-F″)** and TOMM20 **(green; D‴-F‴)** of untreated **(D)**, treated with A$\beta_{25\text{-}35}$ **(E)** or with R^7-G-A$\beta_{25\text{-}35}$ peptide **(F)** in Jurkat cells for 24 h. **(G)** Quantitative data show the mean percentage of membrane or mitochondria area co-localized with $\beta_{25\text{-}35}$ epitope sequence in Jurkat cells treated with R^7-G-A$\beta_{25\text{-}35}$ (200 μM) peptide. **(H)** Representative images show the measurement of total and co-localized area. The numbers represent the mean percentage of three independent experiments. *$p<0.05$; **$p<0.01$; ***$p<0.001$. Image magnification 100x. . (For interpretation of the references to colour in this figure legend, the reader is referred to the Web version of this article.)

3.6. The R^7-G-A$\beta_{25\text{-}35}$ peptide is innocuous to non-leukemic proliferative stromal cells

To test the selective effect of R^7-G-A$\beta_{25\text{-}35}$ peptide on normal non-leukemic proliferative cells, we left mesenchymal stromal cells (MSC) untreated or incubated with A$\beta_{25\text{-}35}$ or R^7-G-A$\beta_{25\text{-}35}$ peptides (200 μM) for 24 h, and evaluated the ΔΨm, ROS production and cell cycle analysis by flow cytometry and fluorescent microscopy (FM). Flow cytometry and FM analysis reveal that, like untreated cells (Fig. 6A and D, 6E″), neither A$\beta_{25\text{-}35}$ (Fig. 6B, D, 6F″) nor R^7-G-A$\beta_{25\text{-}35}$ (Fig. 6C, D, 6G")

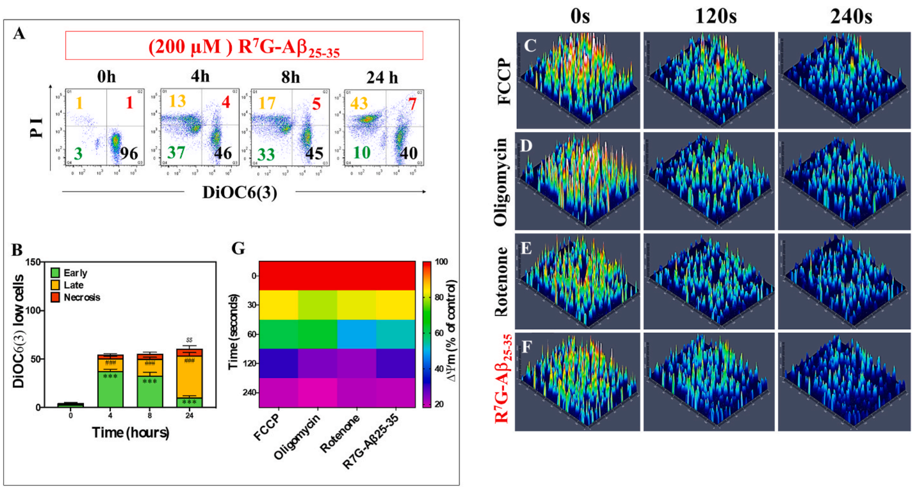

Fig. 5. Fast depolarization of mitochondrial membrane potential (ΔΨm) by synthetic peptide R^7-G-Aβ$_{25-35}$ in Jurkat cells.
(A) Representative dot plot show DiOC$_6$ (3) /PI double staining in Jurkat cells treated with R^7G-Aβ$_{25-35}$ peptide (200 µM) for 0, 4, 8, and 24 h. **(B)** Quantitative data show the mean percentage of early (DiOC$_6$ (3)^{low}/PI$^-$; Q4) and late (DiOC$_{(6)}$3^{low}/PI$^+$; Q1) apoptotic cells, or the necrotic (DiOC$_6$ (3)^{high}/PI$^+$; Q2) population. **(C–F)** Representative spectral images show the fluorescence intensity of Jurkat cells treated with **(C)** FCCP (10 µM), **(D)** Oligomycin (5 µg/ml), **(E)** rotenone (100 µM), and **(F)** R^7G-Aβ$_{25-35}$ peptide (200 µM) during 0, 120 and 240 s. **(G)** Heat map shows the mean fluorescence intensity (% of control at 0 s) of DiOC$_6$ (3) in Jurkat cells treated with FCCP (10 µM), oligomycin (5 µg/ml), rotenone (100 µM), or R^7-G-Aβ$_{25-35}$ peptide (200 µM) during 0, 30, 60, 120 and 240 s. The numbers represent the mean percentage of three independent experiments. *$p<0.05$; **$p<0.01$; ***$p<0.001$.* Image magnification 20x.

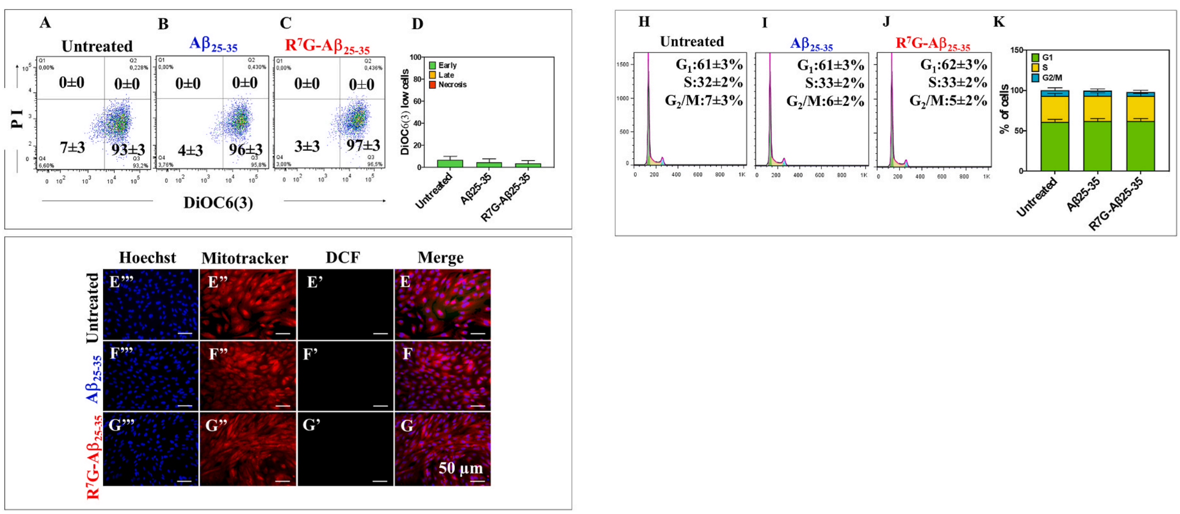

Fig. 6. Synthetic peptide R^7-G-Aβ$_{25-35}$ induces no mitochondrial membrane potential (ΔΨm) dissipation, reactive oxygen species (ROS) production or cell cycle arrest in normal proliferative cells mesenchymal stromal cells (MSCs).
(A) Representative dot plot show DiOC$_6$(3)/PI double staining in MSCs untreated or treated with Aβ$_{25-35}$ (200 µM) or R^7-G-Aβ$_{25-35}$ (200 µM) peptides for 24 h. **(B)** Quantitative data show the DiOC$_6$(3)^{low} mean percentage (Q1 + Q4) of MSCs untreated or treated Aβ$_{25-35}$ and R^7-G-Aβ$_{25-35}$ (200 µM) peptides. **(C–E)** Representative merge fluorescence images show DCF **(C′-E′)**, Mitotracker **(C″-E″)** and Hoechst **(C‴-E‴)** staining in MSCs untreated **(C)**, treated with Aβ$_{25-35}$ **(D)** or R^7-G-Aβ$_{25-35}$ **(E)** peptides for 24 h. **(F)** Representative histograms show cell cycle phase in MSCs untreated or treated with Aβ$_{25-35}$ or R^7-G-Aβ$_{25-35}$ (200 µM) synthetic peptides for 24 h. **(G)** Quantitative data show the cell cycle phase mean percentage of MSCs treated as described above. Figures represent 1 out of 3 independent experiments. The numbers represent the mean percentage of three independent experiments. *$p<0.05$; **$p<0.01$; ***$p<0.001$.* Image magnification 20x.

peptides affected ΔΨm (Fig. 6A–G). Further, the peptides neither induced ROS production (Fig. 6F’ and 6G’) nor affected the cell cycle progression in MSC (Fig. 6I–K) compared to untreated cells (Fig. 6H, K, and 6E′).

4. Discussion

Cell-penetrating peptides (C-PP) are promising anti-cancer agents [18,25]. Here, we report for the first time that the synthetic cationic peptide R^7-G-Aβ$_{25-35}$ and Aβ$_{25-35}$-G-R^7, but not Aβ$_{25-35}$ peptide, induced cell death in Jurkat cells, albeit with different strengths. Effectively, the R^7-G-Aβ$_{25-35}$ reduced cellular metabolic activity (e.g., −25 to −48% reduction), induced G2/M-phase cell arrest (15–20%), and reduced cell proliferation (−74% reduction). Why is R^7-G-Aβ$_{25-35}$ more cytotoxic than Aβ$_{25-35}$-G-R^7? One possible explanation is that the poly-R^7 located at the amino-terminal of the Aβ$_{25-35}$ might provide a better cell-penetrating capability of the peptide through a passive translocation mechanism [22] than when the poly-R^7 is located at the carboxyl-terminal position of the Aβ$_{25-35}$. Interestingly, we found that the Aβ$_{25-35}$ peptide was innocuous to Jurkat cells. This observation might be the result of significant differences in the net charge (at pH:7.0) between the Aβ$_{25-35}$ fragment (+1.00) and R^7-G-Aβ$_{25-35}$ (+8.00). Indeed, the high net charge of the poly-R-peptide might favor its faster interaction with the highly negative charge of the cellular plasma membrane (∼−60 mV), thereby facilitating its cell entrance. Together these observations suggest that the poly-R^7 attached to the amino position is critical for efficient cell-penetrating peptide. However, further chemical structural studies are needed (e.g., circular dichroism spectroscopy) to fully understand the biochemical behavior of the R^7-G-Aβ$_{25-35}$ (Aβ$_{25-35}$-G-R^7) peptide. Whatever the mechanism of interaction between poly-R^7 peptides and plasma membrane, we found that once inside the cell, the R^7-G-Aβ$_{25-35}$ targets mitochondria.

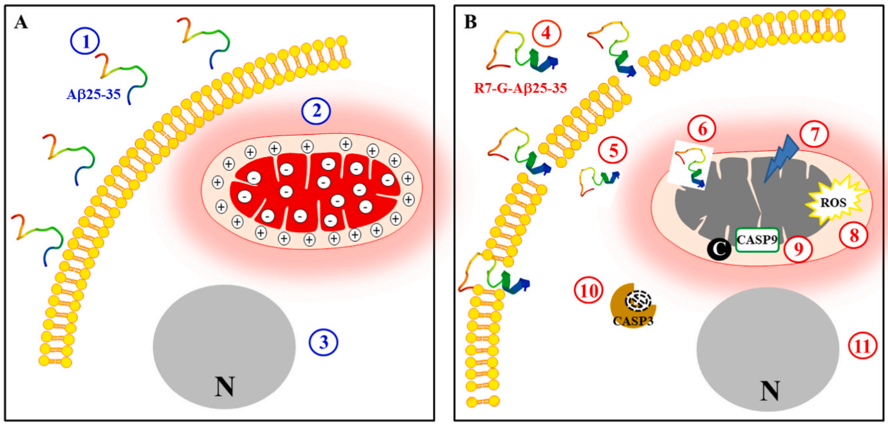

Fig. 7. Schematic representation of the cytotoxic effect of R^7-G-A$\beta_{25\text{-}35}$ on Jurkat cells.
(See text for explanation).

Mounting evidence has shown that mitochondria play a central role in the regulation of cellular metabolism, bioenergetics, and cell life/death decision during carcinogenesis [44]. Therefore, therapeutic interventions (e.g., mitocans) for the targeting of mitochondria exhibit enormous potential for future leukemia therapeutic strategies [20]. In line with this view, we show that R^7-G-A$\beta_{25\text{-}35}$ induced a rapid depolarization of the $\Delta\Psi_m$ as early as 240s post-exposure in Jurkat cells. Remarkably, the R^7-G-A$\beta_{25\text{-}35}$ -induced loss of $\Delta\Psi_m$ resembled the rapid depolarization of the mitocan 5 rotenone, which specifically blocks mitochondrial complex I, and of the mitocan 5 oligomycin, which specifically blocks F_o of the ATP synthase [19]. These observations suggest that R^7-G-A$\beta_{25\text{-}35}$ might work as mitocan 5. However, whether R^7-G-A$\beta_{25\text{-}35}$ directly interacts with mitochondrial complex I and/or ATP synthase, or if the mitochondrial depolarization is the consequence of the interaction of the poly-R^7 peptide with the outer mitochondria membrane requires further investigation. However, since R^7-G-A$\beta_{25\text{-}35}$ -induced mitochondrial depolarization also resembled the effect of the uncoupler FCCP, our observations favor the view that loss of $\Delta\Psi_m$ might be the result of a complex interaction of the peptide with the inner mitochondrial membrane leading to uncoupling mitochondria [45], thereby inhibiting the complex I and ATP synthase, and generating ROS. This assumption is supported by 3 observations. First, R^7-G-A$\beta_{25\text{-}35}$ accumulated at the outer mitochondria membrane according to colocalization with protein TOMM20. However, whether TOMM20 -a mitochondrial import receptor translocase [46] participates in the import of R^7-G-A$\beta_{25\text{-}35}$ to the mitochondrial matrix needs further investigation. Second, R^7-G-A$\beta_{25\text{-}35}$ induced an important production of ROS concomitant with mitochondrial depolarization, an effect that was not reversed by the antioxidant/cytoprotectant NAC [42,43]. Third, it is well established that a drastic loss of $\Delta\Psi_m$ generates ROS [47]. Taken together these observations suggest that R^7-G-A$\beta_{25\text{-}35}$ induces a deleterious domino-like phenomenon in Jurkat cells, involving its accumulation at and ensuing depolarization of mitochondria through uncoupling mechanism, subsequent inhibition of Complex I, generation of ROS, and dysfunction of ATP synthase.

Unexpectedly, we found that the R^7-G-A$\beta_{25\text{-}35}$ peptide did not induce CASPASE-3 activity, thus preserving nucleus integrity [48,49]. We speculate that this phenomenon might be due to the rapid depolarization of mitochondria, which in turn might trap effector cytochrome C, and pro-CASPASE-9 between the inner and outer mitochondria membrane space akin to "Venus's flytrap" mechanism, and depletion of ATP content, thus disabling the apoptosome complex to process pro-CASPASE-3 into active CASPASE-3 [50]. Of note, the specific inhibitor caspase-3 NCSI was unable to protect Jurkat cells against R^7-G-A$\beta_{25\text{-}35}$-induced toxicity. These results imply that R^7-G-A$\beta_{25\text{-}35}$ can kill leukemia cells independently of CASPASE-3 [51]. In contrast to the above observations, R^7-G-A$\beta_{25\text{-}35}$ was innocuous to MenSC –normal non-leukemic proliferative cells. These data suggest that R^7-G-A$\beta_{25\text{-}35}$ specifically deletes leukemia cells.

5. Conclusion

We demonstrate that R^7-G-A$\beta_{25\text{-}35}$ (A$\beta_{25\text{-}35}$-G-R^7) specifically induces cell death in Jurkat cells through a direct and fast disruption of the mitochondria membrane potential, and CASPASE-3 independent mechanism. In agreement with our observations, others have reported that C-PP (e.g., r7-kla; RRRRRRR-GG-IYLATALAKWALKQGF) were able to kill cancer cell lines, including Jurkat cells through permeabilization of the mitochondrial inner membrane, and apoptosis [17,23]. These observations comply with the notion that some C-PP affect mitochondria membranes rather than other cellular membranes. Accordingly, the unmodified A$\beta_{25\text{-}35}$ (Fig. 7, **s**tep **1**) is unable to pass the cellular plasma membrane. Therefore, functional mitochondria (**s2**) and intact nuclei are observed in Jurkat cells (**s3**). In contrast, when cells are exposed to R^7-G-A$\beta_{25\text{-}35}$ peptide (**s4**), it translocates passively to the cell cytoplasm (**s5**). Due to its high net charge (+8.0), the peptide is attracted by the high negative mitochondrial potential (−140 to −180 mV [52]), leading to extensive accumulation of poly-R^7 cation within mitochondria (**s6**) probably with the assistance of protein TOMM20. These actions can disrupt mitochondria membrane integrity, respiration, and ATP synthesis (**s7**), thereby generating a high amount of ROS (**s8**). As a result of those mitochondria alterations, depolarized mitochondria instantly trap pro-apoptogenic proteins pro-caspase-9 and cytochrome C (**s9**) avoiding activation of CASPASE-3 (**s10**). Therefore, despite mitochondria dysfunction, no nuclei damage is appreciably detected (**s11**). Taken together these observations suggest that the cationic Aβ peptide might be a potential anti-leukemia agent against ALL.

Ethical approval and consent to participate

Not applicable.

Consent for publication

Not applicable.

Availability of supporting data

All relevant data and materials are within the paper.

Funding

This research was supported by funding from "Fundación Alfonso Moreno Jaramillo" grant no. #2020–31631. The funders had no role in the study design, data collection, analysis, decision to publish, or preparation of the manuscript.

Authors' contributions

Conceptualization, C.V.-P., and M.J.-Del-R.; methodology, C.V.-P.; validation, M.M.-P.; formal analysis, M.M.-P., and C.V.-P.; investigation, M.M.-P.; resources; C.V.-P. and M.J.-Del-R.; data curation, C.V.-P.; writing—original draft preparation, C.V.-P., and M.J.-Del-R.; writing—review and editing, M.M.-P.; C.V.-P. and M.J-Del-R.; supervision, C.V.-P., and M.J.-Del-R.; project administration, M.J.-Del-R.; funding acquisition, C.V.-P. All authors have read and agreed to the published version of the manuscript.

Declaration of competing interest

All the authors have no competing interests to declare. The funders of the study had no role in study design, data collection, data analysis, data interpretation, or writing of the report.

Acknowledgments

The authors thank the "Fundación Alfonso Moreno Jaramillo" for financial support. We thank Dr. S Estrada-Gomez and CF Salinas-Restrepo (Ofidism/Escorpionism Program, Universidad de Antioquia) for providing the peptide.

References

[1] F. Malard, M. Mohty, Acute lymphoblastic leukemia, Lancet 395 (2020) 1146–1162, https://doi.org/10.1016/S0140-6736(19)33018-1.
[2] Y. Dong, O. Shi, Q. Zeng, X. Lu, W. Wang, Y. Li, Q. Wang, Leukemia incidence trends at the global, regional, and national level between 1990 and 2017, Exp. Hematol. Oncol. 9 (2020) 14, https://doi.org/10.1186/s40164-020-00170-6.
[3] H. Inaba, C.G. Mullighan, Pediatric acute lymphoblastic leukemia, Haematologica 105 (2020) 2524–2539, https://doi.org/10.3324/haematol.2020.247031.
[4] S. Gregory, Adult acute lymphoblastic leukemia: treatment and management updates, Semin. Oncol. Nurs. 35 (2019), 150951, https://doi.org/10.1016/j.soncn.2019.150951.
[5] M. Kato, A. Manabe, Treatment and biology of pediatric acute lymphoblastic leukemia, Pediatr. Int. 60 (2018) 4–12, https://doi.org/10.1111/ped.13457.
[6] K.J. August, E.M. Guest, K. Lewing, J.A. Hays, A.S. Gamis, Treatment of children with relapsed and refractory acute lymphoblastic leukemia with mitoxantrone, vincristine, pegaspargase, dexamethasone, and bortezomib, Pediatr. Blood Cancer 67 (2020), e28062, https://doi.org/10.1002/pbc.28062.
[7] H. Rafei, H.M. Kantarjian, E.J. Jabbour, Targeted therapy paves the way for the cure of acute lymphoblastic leukaemia, Br. J. Haematol. 188 (2020) 207–223, https://doi.org/10.1111/bjh.16207.
[8] L. Galluzzi, I. Vitale, S.A. Aaronson, J.M. Abrams, D. Adam, P. Agostinis, E. S. Alnemri, L. Altucci, I. Amelio, D.W. Andrews, M. Annicchiarico-Petruzzelli, A. V. Antonov, E. Arama, E.H. Baehrecke, N.A. Barlev, N.G. Bazan, F. Bernassola, M.J. M. Bertrand, K. Bianchi, M.V. Blagosklonny, K. Blomgren, C. Borner, P. Boya, C. Brenner, M. Campanella, E. Candi, D. Carmona-Gutierrez, F. Cecconi, F.K. Chan, N.S. Chandel, E.H. Cheng, J.E. Chipuk, J.A. Cidlowski, A. Ciechanover, G. M. Cohen, M. Conrad, J.R. Cubillos-Ruiz, P.E. Czabotar, V. D'Angiolella, T. M. Dawson, V.L. Dawson, V. De Laurenzi, R. De Maria, K.M. Debatin, R. J. DeBerardinis, M. Deshmukh, N. Di Daniele, F. Di Virgilio, V.M. Dixit, S.J. Dixon, C.S. Duckett, B.D. Dynlacht, W.S. El-Deiry, J.W. Elrod, G.M. Fimia, S. Fulda, A. J. Garcia-Saez, A.D. Garg, C. Garrido, E. Gavathiotis, P. Golstein, E. Gottlieb, D. R. Green, L.A. Greene, H. Gronemeyer, A. Gross, G. Hajnoczky, J.M. Hardwick, I. S. Harris, M.O. Hengartner, C. Hetz, H. Ichijo, M. Jaattela, B. Joseph, P.J. Jost, P. P. Juin, W.J. Kaiser, M. Karin, T. Kaufmann, O. Kepp, A. Kimchi, R.N. Kitsis, D. J. Klionsky, R.A. Knight, S. Kumar, S.W. Lee, J.J. Lemasters, B. Levine, A. Linkermann, S.A. Lipton, R.A. Lockshin, C. Lopez-Otin, S.W. Lowe, T. Luedde, E. Lugli, M. MacFarlane, F. Madeo, M. Malewicz, W. Malorni, G. Manic, J. C. Marine, S.J. Martin, J.C. Martinou, J.P. Medema, P. Mehlen, P. Meier, S. Melino, E.A. Miao, J.D. Molkentin, U.M. Moll, C. Munoz-Pinedo, S. Nagata, G. Nunez, A. Oberst, M. Oren, M. Overholtzer, M. Pagano, T. Panaretakis, M. Pasparakis, J. M. Penninger, D.M. Pereira, S. Pervaiz, M.E. Peter, M. Piacentini, P. Pinton, J.H. M. Prehn, H. Puthalakath, G.A. Rabinovich, M. Rehm, R. Rizzuto, C.M. P. Rodrigues, D.C. Rubinsztein, T. Rudel, K.M. Ryan, E. Sayan, L. Scorrano, F. Shao, Y. Shi, J. Silke, H.U. Simon, A. Sistigu, B.R. Stockwell, A. Strasser, G. Szabadkai, S. W.G. Tait, D. Tang, N. Tavernarakis, A. Thorburn, Y. Tsujimoto, B. Turk, T. Vanden Berghe, P. Vandenabeele, M.G. Vander Heiden, A. Villunger, H.W. Virgin, K. H. Vousden, D. Vucic, E.F. Wagner, H. Walczak, D. Wallach, Y. Wang, J.A. Wells, W. Wood, J. Yuan, Z. Zakeri, B. Zhivotovsky, L. Zitvogel, G. Melino, G. Kroemer, Molecular mechanisms of cell death: recommendations of the nomenclature committee on cell death, Cell Death Differ. 25 (2018) 486–541, https://doi.org/10.1038/s41418-017-0012-4, 2018.
[9] B.A. Carneiro, W.S. El-Deiry, Targeting apoptosis in cancer therapy, Nat. Rev. Clin. Oncol. 17 (2020) 395–417, https://doi.org/10.1038/s41571-020-0341-y.
[10] A. Giacometti, O. Cirioni, M.S. Del Prete, A.M. Paggi, M.M. D'Errico, G. Scalise, Combination studies between polycationic peptides and clinically used antibiotics against Gram-positive and Gram-negative bacteria, Peptides 21 (2000) 1155–1160, https://doi.org/10.1016/s0196-9781(00)00254-0.
[11] Y. Zhou, Y. Peng, Synergistic effect of clinically used antibiotics and peptide antibiotics against Gram-positive and Gram-negative bacteria, Exp. Ther. Med. 6 (2013) 1000–1004, https://doi.org/10.3892/etm.2013.1231.
[12] S. Omardien, S. Brul, S.A. Zaat, Antimicrobial activity of cationic antimicrobial peptides against gram-positives: current progress made in understanding the mode of action and the response of bacteria, Front. Cell Dev. Biol. 4 (2016) 111, https://doi.org/10.3389/fcell.2016.00111.
[13] Y.X. Li, Z. Zhong, W.P. Zhang, P.Y. Qian, Discovery of cationic nonribosomal peptides as Gram-negative antibiotics through global genome mining, Nat. Commun. 9 (2018) 3273, https://doi.org/10.1038/s41467-018-05781-6.
[14] Y. Huan, Q. Kong, H. Mou, H. Yi, Antimicrobial peptides: classification, design, application and research progress in multiple fields, Front. Microbiol. 11 (2020), 582779, https://doi.org/10.3389/fmicb.2020.582779.
[15] L.T. Nguyen, E.F. Haney, H.J. Vogel, The expanding scope of antimicrobial peptide structures and their modes of action, Trends Biotechnol. 29 (2011) 464–472, https://doi.org/10.1016/j.tibtech.2011.05.001.
[16] C. Segura, F. Guzmán, L.M. Salazar, M.E. Patarroyo, S. Orduz, V. Lemeshko, BTM-P1 polycationic peptide biological activity and 3D-dimensional structure, Biochem. Biophys. Res. Commun. 353 (2007) 908–914, https://doi.org/10.1016/j.bbrc.2006.12.113.
[17] V.V. Lemeshko, Electrical potentiation of the membrane permeabilization by new peptides with anticancer properties, Biochim. Biophys. Acta 1828 (2013) 1047–1056, https://doi.org/10.1016/j.bbamem.2012.12.012.
[18] O.O. Bakare, A. Gokul, R. Wu, L.A. Niekerk, A. Klein, M. Keyster, Biomedical relevance of novel anticancer peptides in the sensitive treatment of cancer, Biomolecules 11 (2021), https://doi.org/10.3390/biom11081120.
[19] J. Neuzil, L.F. Dong, J. Rohlena, J. Truksa, S.J. Ralph, Classification of mitocans, anti-cancer drugs acting on mitochondria, Mitochondrion 13 (2013) 199–208, https://doi.org/10.1016/j.mito.2012.07.112.
[20] L. Dong, V. Gopalan, O. Holland, J. Neuzil, Mitocans revisited: mitochondrial targeting as efficient anti-cancer therapy, Int. J. Mol. Sci. 21 (2020), https://doi.org/10.3390/ijms21217941.
[21] P.A. Wender, D.J. Mitchell, K. Pattabiraman, E.T. Pelkey, L. Steinman, J. B. Rothbard, The design, synthesis, and evaluation of molecules that enable or enhance cellular uptake: peptoid molecular transporters, Proc. Natl. Acad. Sci. U. S. A. 97 (2000) 13003–13008, https://doi.org/10.1073/pnas.97.24.13003.
[22] C. Allolio, A. Magarkar, P. Jurkiewicz, K. Baxová, M. Javanainen, P.E. Mason, R. Šachl, M. Cebecauer, M. Hof, D. Horinek, V. Heinz, R. Rachel, C.M. Ziegler, A. Schröfel, P. Jungwirth, Arginine-rich cell-penetrating peptides induce membrane multilamellarity and subsequently enter via formation of a fusion pore, Proc. Natl. Acad. Sci. U. S. A. 115 (2018) 11923–11928, https://doi.org/10.1073/pnas.1811520115.
[23] B. Law, L. Quinti, Y. Choi, R. Weissleder, C.H. Tung, A mitochondrial targeted fusion peptide exhibits remarkable cytotoxicity, Mol. Cancer Therapeut. 5 (2006) 1944–1949, https://doi.org/10.1158/1535-7163.MCT-05-0509.
[24] C.H. Tung, R. Weissleder, Arginine containing peptides as delivery vectors, Adv. Drug Deliv. Rev. 55 (2003) 281–294, https://doi.org/10.1016/s0169-409x(02)00183-7.
[25] A. Borrelli, A.L. Tornesello, M.L. Tornesello, F.M. Buonaguro, Cell penetrating peptides as molecular carriers for anti-cancer agents, Molecules 23 (2018), https://doi.org/10.3390/molecules23020295.
[26] T. Kubo, S. Nishimura, Y. Kumagae, I. Kaneko, In vivo conversion of racemized beta-amyloid ([D-Ser 26]A beta 1-40) to truncated and toxic fragments ([D-Ser 26]A beta 25-35/40) and fragment presence in the brains of Alzheimer's patients, J. Neurosci. Res. 70 (2002) 474–483, https://doi.org/10.1002/jnr.10391.
[27] H.H. Tsai, J.B. Lee, S.S. Tseng, X.A. Pan, Y.C. Shih, Folding and membrane insertion of amyloid-beta (25-35) peptide and its mutants: implications for aggregation and neurotoxicity, Proteins 78 (2010) 1909–1925, https://doi.org/10.1002/prot.22705.
[28] A.K. Smith, D.K. Klimov, De novo aggregation of Alzheimer's Aβ25-35 peptides in a lipid bilayer, Sci. Rep. 9 (2019) 7161, https://doi.org/10.1038/s41598-019-43685-7.
[29] O.F. Luna, J. Gomez, C. Cárdenas, F. Albericio, S.H. Marshall, F. Guzmán, Deprotection reagents in Fmoc solid phase peptide synthesis: moving away from piperidine? Molecules 21 (2016) https://doi.org/10.3390/molecules21111542.
[30] R.A. Houghten, General method for the rapid solid-phase synthesis of large numbers of peptides: specificity of antigen-antibody interaction at the level of individual amino acids, Proc. Natl. Acad. Sci. U. S. A. 82 (1985) 5131–5135, https://doi.org/10.1073/pnas.82.15.5131.
[31] D. Quintero-Espinosa, V. Soto-Mercado, C. Quintero-Quinchia, M. Mendivil-Perez, C. Velez-Pardo, M. Jimenez-Del-Rio, Latent tri-lineage potential of human menstrual blood-derived mesenchymal stromal cells revealed by specific in vitro

culture conditions, Mol. Neurobiol. 58 (2021) 5194–5209, https://doi.org/10.1007/s12035-021-02442-6.
[32] J. van Meerloo, G.J. Kaspers, J. Cloos, Cell sensitivity assays: the MTT assay, Methods Mol. Biol. 731 (2011) 237–245, https://doi.org/10.1007/978-1-61779-080-5_20.
[33] C. Graefe, L. Eichhorn, P. Wurst, J. Kleiner, A. Heine, I. Panetas, Z. Abdulla, A. Hoeft, S. Frede, C. Kurts, E. Endl, C.K. Weisheit, Optimized Ki-67 staining in murine cells: a tool to determine cell proliferation, Mol. Biol. Rep. 46 (2019) 4631–4643, https://doi.org/10.1007/s11033-019-04851-2.
[34] Y. Shen, P. Vignali, R. Wang, Rapid profiling cell cycle by flow cytometry using concurrent staining of DNA and mitotic markers, Bio. Protoc. 7 (2017), https://doi.org/10.21769/BioProtoc.2517.
[35] G. Rothe, G. Valet, Flow cytometric assays of oxidative burst activity in phagocytes, Methods Enzymol. 233 (1994) 539–548.
[36] L.B. Monteiro, G.G. Davanzo, C.F. de Aguiar, P.M.M. Moraes-Vieira, Using flow cytometry for mitochondrial assays, MethodsX 7 (2020), 100938, https://doi.org/10.1016/j.mex.2020.100938.
[37] R. Fox, M. Aubert, Flow cytometric detection of activated caspase-3, Methods Mol. Biol. 414 (2008) 47–56, https://doi.org/10.1007/978-1-59745-339-4_5.
[38] V.E. Jahnke, O. Sabido, D. Freyssenet, Control of mitochondrial biogenesis, ROS level, and cytosolic Ca2+ concentration during the cell cycle and the onset of differentiation in L6E9 myoblasts, Am. J. Physiol. Cell Physiol. 296 (2009) C1185–C1194, https://doi.org/10.1152/ajpcell.00377.2008.
[39] V. Soto-Mercado, M. Mendivil-Perez, M. Jimenez-Del-Rio, J.E. Fox, C. Velez-Pardo, Cannabinoid CP55940 selectively induces apoptosis in Jurkat cells and in ex vivo T-cell acute lymphoblastic leukemia through H, Leuk. Res. 95 (2020), 106389, https://doi.org/10.1016/j.leukres.2020.106389.
[40] J. Schindelin, I. Arganda-Carreras, E. Frise, V. Kaynig, M. Longair, T. Pietzsch, S. Preibisch, C. Rueden, S. Saalfeld, B. Schmid, J.Y. Tinevez, D.J. White, V. Hartenstein, K. Eliceiri, P. Tomancak, A. Cardona, Fiji: an open-source platform for biological-image analysis, Nat. Methods 9 (2012) 676–682, https://doi.org/10.1038/nmeth.2019.
[41] J. Zhang, X. Wang, V. Vikash, Q. Ye, D. Wu, Y. Liu, W. Dong, ROS and ROS-mediated cellular signaling, Oxid. Med. Cell. Longev. (2016), 4350965, https://doi.org/10.1155/2016/4350965, 2016.
[42] D. Ezeriņa, Y. Takano, K. Hanaoka, Y. Urano, T.P. Dick, N-acetyl cysteine functions as a fast-acting antioxidant by triggering intracellular H, Cell Chem. Biol. 25 (2018) 447–459, https://doi.org/10.1016/j.chembiol.2018.01.011, e444.
[43] B. Pedre, U. Barayeu, D. Ezeriņa, T.P. Dick, The mechanism of action of N-acetylcysteine (NAC): the emerging role of H, Pharmacol. Ther. 228 (2021), 107916, https://doi.org/10.1016/j.pharmthera.2021.107916.
[44] L. Moro, Mitochondria at the crossroads of physiology and pathology, J. Clin. Med. 9 (2020), https://doi.org/10.3390/jcm9061971.
[45] S. Demine, P. Renard, T. Arnould, Mitochondrial uncoupling: a key controller of biological processes in physiology and diseases, Cells 8 (2019), https://doi.org/10.3390/cells8080795.
[46] M. Yano, M. Kanazawa, K. Terada, M. Takeya, N. Hoogenraad, M. Mori, Functional analysis of human mitochondrial receptor Tom20 for protein import into mitochondria, J. Biol. Chem. 273 (1998) 26844–26851, https://doi.org/10.1074/jbc.273.41.26844.
[47] B.J. Berry, A.J. Trewin, A.M. Amitrano, M. Kim, A.P. Wojtovich, Use the protonmotive force: mitochondrial uncoupling and reactive oxygen species, J. Mol. Biol. 430 (2018) 3873–3891, https://doi.org/10.1016/j.jmb.2018.03.025.
[48] R.U. Janicke, M.L. Sprengart, M.R. Wati, A.G. Porter, Caspase-3 is required for DNA fragmentation and morphological changes associated with apoptosis, J. Biol. Chem. 273 (1998) 9357–9360.
[49] M. Woo, R. Hakem, M.S. Soengas, G.S. Duncan, A. Shahinian, D. Kägi, A. Hakem, M. McCurrach, W. Khoo, S.A. Kaufman, G. Senaldi, T. Howard, S.W. Lowe, T. W. Mak, Essential contribution of caspase 3/CPP32 to apoptosis and its associated nuclear changes, Genes Dev. 12 (1998) 806–819, https://doi.org/10.1101/gad.12.6.806.
[50] L. Dorstyn, C.W. Akey, S. Kumar, New insights into apoptosome structure and function, Cell Death Differ. 25 (2018) 1194–1208, https://doi.org/10.1038/s41418-017-0025-z.
[51] L. Lartigue, Y. Kushnareva, Y. Seong, H. Lin, B. Faustin, D.D. Newmeyer, Caspase-independent mitochondrial cell death results from loss of respiration, not cytotoxic protein release, Mol. Biol. Cell 20 (2009) 4871–4884, https://doi.org/10.1091/mbc.e09-07-0649.
[52] L.D. Zorova, V.A. Popkov, E.Y. Plotnikov, D.N. Silachev, I.B. Pevzner, S. S. Jankauskas, V.A. Babenko, S.D. Zorov, A.V. Balakireva, M. Juhaszova, S. J. Sollott, D.B. Zorov, Mitochondrial membrane potential, Anal. Biochem. 552 (2018) 50–59, https://doi.org/10.1016/j.ab.2017.07.009.